JOURNAL OF THERMOPHYSICS AND HEAT TRANSFER
Vol. 22, No. 4, October–December 2008

Spectroscopic Flow Evaluation in Inductively Coupled Plasma Wind Tunnel

Kazuhisa Fujita,* Masahito Mizuno,† Kiyomichi Ishida,‡ and Takeshi Ito§
Japan Aerospace Exploration Agency, Tokyo 182-8522, Japan

DOI: 10.2514/1.34032

Radiation spectroscopy of high-enthalpy flows in a 110-kW-class inductively coupled plasma wind tunnel is conducted to improve the accuracy of the radiation code and to measure the flow properties in the test section of the wind tunnel in detail. Imaging spectroscopy is done to obtain radial profiles of emission spectra at a single moment, from which the radial distribution of the emission intensity is determined by the inverse Abel conversion. The molecular temperature and the chemical species concentration are determined by the spectrum fitting method through the use of the radiation code, SPRADIAN2. To accomplish better agreement between the numerical predictions and experiments, the theoretical model and the spectroscopic data for the radiation code are replaced with more accurate data to reflect the recent experimental and theoretical results. As a result, the radial distributions of the temperature, the concentration of the impurities as well as the major chemical components, and the flow enthalpy are accurately determined for nitrogen and air flows in the test section of the wind tunnel.

I. Introduction

RADIATION spectroscopy is one of the powerful tools used to measure the thermodynamic properties of high-enthalpy flows. It is often more favorable than other diagnostic techniques because it allows us to keep flows undisturbed without any insertion of probes into the flow [1,2]. However, it is often difficult to directly measure the flow properties from the observed emission, because radiation from a high-temperature gas is produced as a result of complex physical processes in the flow. That is, the emission spectrum essentially depends on the chemical species concentration and the internal level population, which are determined as a result of chemical reactions and thermal relaxation, respectively.

With regard to atomic species, it is not difficult to determine the relative level population of electronic states from individual atomic line intensities, because atomic lines can be distinctively measured apart from other spectral lines and continua. In contrast to this, it is more difficult to determine the level population for molecular species, especially when the spectral resolution is not so high, because individual rotational lines merge and form a series of band spectra as a whole. To determine the molecular level population or temperature, it is necessary to use the trial and error method in such a way that the emission spectrum is computed by changing the level population and the species concentration until the observed spectrum can be numerically reproduced. This is the so-called molecular spectrum fitting method. Because the accuracy of the rotational and vibrational temperatures so determined is expected to depend on the accuracy of the analytical model and the numerical procedure used to compute the emission spectrum, it is necessary to use an accurate radiation code for the temperature measurement.

In previous studies, the authors developed a line-by-line radiation code, SPRADIAN [3], which was applied to assess the radiative heat transfer rate of the HAYABUSA sample return capsule reentering the Earth's atmosphere at a hyperbolic velocity [4] and to measure the rotational and vibrational temperatures of N_2 and N_2^+ behind a strong shock wave using the molecular spectrum fitting method [5]. In both studies, because the required spectral resolution was not so high, spin splitting of molecular multiplet states was not incorporated into the model. The molecular rovibrational level was described by the power series of the rotational and vibrational quantum numbers with only low-order terms using the spectroscopic constants T_e, ω_e, $\omega_e x_e$, $\omega_e y_e$, $\omega_e z_e$, B_e, and α_e. In addition to these simplifications, the accuracy of SPRADIAN has not been sufficiently validated by spectroscopic measurements.

Recently, in an attempt to improve SPRADIAN for the purpose of molecular spectroscopy with high spectral resolution and radiation analysis of the planetary atmospheric entry with ablation of the thermal protection system (TPS) involved, the spectroscopic database has been updated with the additional atomic and molecular species. The analytical model has been improved to take into account spin splitting of multiplet states. In this paper, the accuracy of the improved version, SPRADIAN2, is validated by the spectroscopic measurement using an inductively coupled plasma (ICP) wind tunnel as a quasi-stationary plasma source. Finally, the flow properties in the test section of the ICP wind tunnel are determined in detail.

II. Experimental Procedure

A. Inductively Coupled Plasma Wind Tunnel

The present measurement was conducted in a 110-kW-class ICP wind tunnel, which was recently developed at the Aerospace Research Center, Japan Aerospace Exploration Agency [6]. The experimental setup is schematically illustrated in Fig. 1. The ICP heater has a cylindrical discharge chamber made of quartz glass with a 75 mm inner diameter, which is covered by an outer sleeve made of quartz glass to form a cooling water jacket of 2 mm in thickness between them. The heater operates by supplying 1.78 MHz radio-frequency current to the three-turn induction coil up to 110 kW of power. In the typical operation at 90 kW, the operational mass flow rate of the air can be changed from 1.5 to 2.0 g/s. The thermal efficiency deduced from the thermal balance of the heater is estimated to be 30%, realizing the test flow enthalpy of 14–18 MJ/kg. The heater is horizontally mounted to the vacuum chamber in which the ambient pressure is controlled. The heater can operate at ambient pressures from 1 to 10 kPa, depending on the gas flow rate and the electric input power. More detailed information may be found in [6].

In comparison with the arc-heated wind tunnel, the primary advantage of the ICP wind tunnel is that it can produce a

Presented as Paper 0173 at the 43rd AIAA Aerospace Science Meeting and Exhibit, Reno, Nevada, 10–13 January 2005; received 14 August 2007; revision received 5 May 2008; accepted for publication 6 May 2008.

*Doctor of Engineering, Senior Researcher, Institute of Aerospace Technology, 7-44-1 Jinidaiji-higashi-machi, Chofu; kazudom@chofu.jaxa.jp. Senior Member AIAA.
†Doctor of Engineering, Researcher.
‡Senior Researcher.
§Doctor of Engineering, Senior Researcher. Senior Member AIAA.

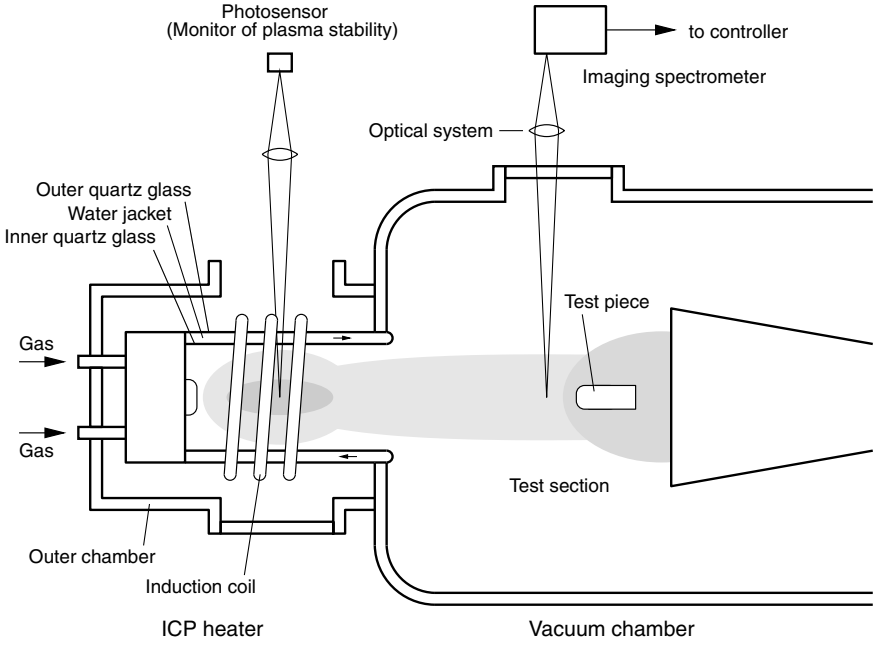

Fig. 1 Schematic view of the experimental setup.

high-enthalpy flow with less contamination of eroded electrode materials, because the working gas is heated by electrodeless discharge. Such a characteristic is favorable for the evaluation of TPS performance and assessment of the surface catalysis of the TPS material [6]. In addition to this primary advantage, the ICP wind tunnel can work as a good plasma source, generating a quasi-stationary and local-thermochemical-equilibrium (LTE) plasma in the downstream region of the heater, because the flow in the test section is low subsonic and the pressure remains sufficiently high without nozzle expansion (see Fig. 1). This allows us to concentrate our attention on only the radiation mechanism instead of the chemical kinetics and the thermal relaxation in the spectroscopic measurements.

B. Imaging Spectroscopy

In the present measurement, one-dimensional imaging spectroscopy was conducted to obtain the radial distribution of the emission spectrum from the test flow. A one-dimensional radial image of the radiating gas is focused by a quartz lens on an objective slit of the spectrometer and then separated into its spectral components by an Acton SpectraPro 500i imaging spectrometer, generating a spatial vs spectral image on the photosensitive surface of an ANDOR DH520 image-intensified charge-coupled device (ICCD) camera attached to the spectrometer. To increase the signal-to-noise ratio, the spatial components of the ICCD pixels are accumulated at an interval of every 7 pixels to form a multiband image. This realizes a 1.60 mm spatial resolution in the radial direction at the center of the test flow. The imaging spectroscopy is performed in the wavelength range of 200–900 nm. An overall spectrum is constructed from eight individual images that cover 200–300, 300–400, 350–450, 450–550, 550–650, 650–750, 750–850, and 800–900 nm wavelengths, respectively. The spectroscopic system is calibrated as a whole by using an Optronic Laboratories UV-40IR deuterium lamp and a 550 C standard tungsten lamp.

Because the overall spectrum is constructed from the eight individual spectra, the accuracy of the overall spectrum is subject to the stability and reproducibility of the plasma source during the operation. To check the stability of plasma in the discharge chamber, a Hamamatsu Photonics C6386 photosensor with a 20 MHz response was used to monitor the total intensity of light emitted from the coil center where heat generation is the most intense, in addition to accurately controlling the input power, the gas flow rate, and the ambient pressure in the test section. A typical example of the output signal from the photosensor and the frequency distribution obtained by a fast Fourier transform analyzer is shown in Fig. 2. In general, the emission from the coil center is satisfactorily stable with a fluctuation of less than 5% in the operational power range, and the fluctuation increases as the input power decreases out of the operational power range. The signal contains noises at 50 Hz and overtone frequencies, as seen in Fig. 2b. These noises originate from the ac power supplied to the power unit of the ICP heater. A noise frequency of 1.78 MHz observed in Fig. 2c corresponds to the resonance frequency of the electric circuit in the power unit.

From these measurements, the test flow produced by the ICP heater can be regarded as a quasi-stationary plasma as long as the measurements are made on a time scale sufficiently longer than 20 ms. To fulfill this requirement, the exposure time of the ICCD camera was set to 200 ms to obtain a time-averaged spectrum. A series of spectroscopy from the short to long wavelength ranges was repeated 10 times to produce an average spectrum. In general, deviation of an individual spectrum from the average remains less than 3% over the entire wavelength range.

III. Radiation Code

In the present study, an improved version of the radiation code SPRADIAN, named SPRADIAN2, was used to compute a numerical spectrum. SPRADIAN is a multipurpose software package for radiation analysis [3], used not only to compute emission and absorption coefficients in a line-by-line manner [7] but also to perform multidimensional radiative heat transfer calculations [4,8]. The bound–free and free–free electronic transitions are taken into account as well to produce a realistic numerical spectrum containing continua. A detailed description of the radiation theory, the mathematical model, and the numerical procedure incorporated into SPRADIAN is given in [3]. Problems in the old version of SPRADIAN are that 1) spin splitting of multiplet states is not accurately taken into account; 2) the rovibrational level is expressed by the power series of the rotational and vibrational quantum numbers with only low-order terms using the spectroscopic constants, T_e, ω_e, $\omega_e x_e$, $\omega_e y_e$, $\omega_e z_e$, B_e, and α_e; 3) the chemical species included in the database are not sufficient for widespread application; and 4) code verification by means of experiment has not been done. In SPRADIAN2, these problems are reasonably settled as described herein.

In most applications, unless a spectrum with great resolution is concerned, lambda-type doubling has little influence on the spectrum

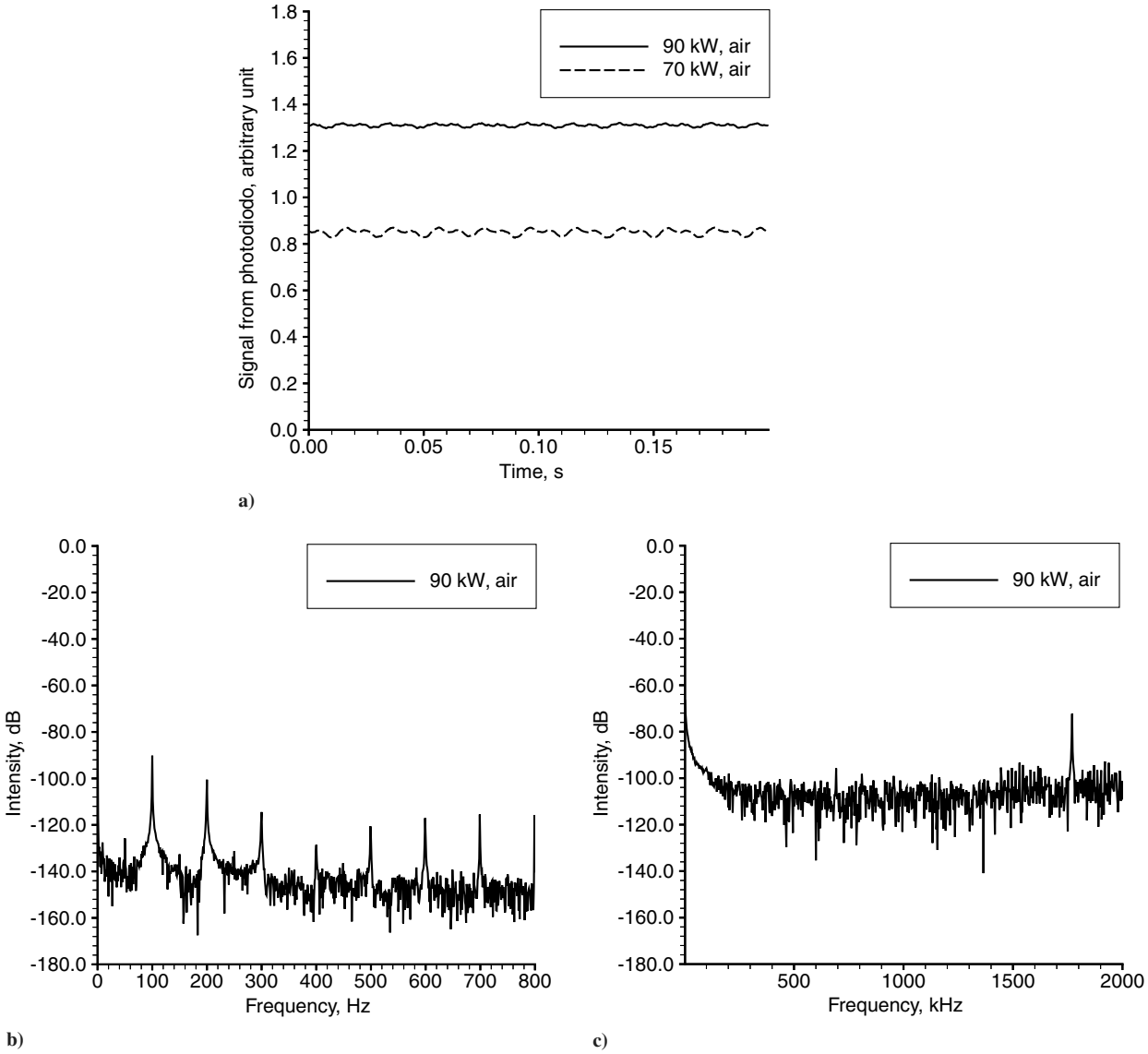

Fig. 2 Fluctuation of the total radiation intensity measured at the coil center: a) output signals of the photosensor at a low time resolution, and frequency distribution in a b) low, and c) high frequency range, respectively.

shape [9]. For this reason, the lambda-type doubling is left neglected in SPRADIAN2 as before. Because the spin splitting in $\Sigma \leftrightarrow \Sigma$ transitions is negligibly small, these transitions are uniquely regarded as the ${}^1\Sigma \leftrightarrow {}^1\Sigma$ transition without the spin splitting. Consequently, the electronic transitions of ${}^2\Pi \leftrightarrow {}^2\Sigma$, ${}^3\Pi \leftrightarrow {}^3\Sigma$, ${}^1\Pi \leftrightarrow {}^1\Pi$, ${}^2\Pi \leftrightarrow {}^2\Pi$, and ${}^3\Pi \leftrightarrow {}^3\Pi$ are newly incorporated into SPRADIAN2, following the mathematical model described in [9]. However, in the preliminary calculations, the spin splitting in the $\Pi \leftrightarrow \Pi$ transitions was found to have little influence on the spectrum shape at a moderate spectral resolution. For this reason, for the purpose of reducing the computational time, the $\Pi \leftrightarrow \Pi$ transitions are allowed to be replaced with the ${}^1\Sigma \leftrightarrow {}^1\Sigma$ transition according to user's intension.

The database of SPRADIAN2 currently includes 13 atomic species (H, He, C, N, O, Ne, Ar, He^+, C^+, N^+, O^+, Ne^+, and Ar^+) and 12 molecular species (H_2, C_2, N_2, O_2, N_2^+, CH, NH, OH, CN, CO, CO^+, and NO) with 37 electronic transitions (for details, see [10]). Intense band spectra of hydrides and carbonic species are newly added in this study to cope with the unresolved band spectra observed in the previous measurement [11]. To numerically reproduce the experimental spectrum emitted from the air and nitrogen test flows containing impurities, the gas species and the electronic transitions shown in Table 1 are taken into consideration in this study. The atomic energy levels and the transition probabilities of H are taken from [12], and those of C, N, O, C^+, N^+, and O^+ are taken from [13]. On the other hand, the rotational–vibrational–electronic transition probability of the molecular species is computed using the spectroscopic constant and the electronic transition moment taken from the references listed in Table 1. The rovibrational level is expressed with higher-order terms, that is, the vibrational term, T_v, is given by a seventh-order polynomial of $(v + 1/2)$, whereas the rotational constants, B_v and D_v, are expressed in a polynomial expression of the fifth and the second orders, respectively.

IV. Experimental Results

A. Overall Spectrum

In the present measurement, the ICP heater was operated at the input power of 90 kW while maintaining the ambient pressure at 10 kPa in the test section. Nitrogen and air were used as the working gases. The flow rate of nitrogen and air supplied to the ICP heater was set to 1.7 and 1.8 g/s, respectively. Radial imaging spectroscopy of the test flow was performed in the test section at a 592 mm distance downstream from the coil center. A typical example of the radial imaging spectrum from 350 to 450 nm is shown in Fig. 3. In this case, the imaging spectrum consisted of 36 individual spectra at every 1.60 mm radial position. Taking an average over 10 imaging spectra,

Table 1 Gas species and electronic transitions taken into consideration to compute a numerical spectrum for air and nitrogen test flows containing impurities

Spectrum type	Species	References
Atomic lines	H, C, N, O, C^+, N^+, O^+	[12,13]
Molecular bands	N_2 ($A \leftrightarrow X$, $B \leftrightarrow A$, $C \leftrightarrow B$, $a \leftrightarrow X$, $b \leftrightarrow X$, $b' \leftrightarrow X$)	[14–16]
	O_2 ($B \leftrightarrow X$)	[14–16]
	N_2^+ ($A \leftrightarrow X$, $B \leftrightarrow X$, $C \leftrightarrow X$)	[14–16]
	CH ($A \leftrightarrow X$, $B \leftrightarrow X$)	[14,17–19]
	NH ($A \leftrightarrow X$, $c \leftrightarrow a$, $c \leftrightarrow b$)	[14,20–23]
	OH ($A \leftrightarrow X$)	[14,24,25]
	CN ($A \leftrightarrow X$, $B \leftrightarrow X$)	[14,26–28]
	NO ($A \leftrightarrow X$, $B \leftrightarrow X$, $C \leftrightarrow X$, $D \leftrightarrow X$)	[14,29–32]
Bound–free continua	$H + h\nu \leftrightarrow H^+ + e$	[3]
	$C + h\nu \leftrightarrow C^+ + e$	[3]
	$N + h\nu \leftrightarrow N^+ + e$	[3]
	$O + h\nu \leftrightarrow O^+ + e$	[3]
	$O^- + h\nu \leftrightarrow O + e$	[3]
Free–free continua [a]	N_2, N, O, and arbitrary ions	[3]

[a]The species of free–free continua is substituted with the ones accelerating electrons effectively

an averaged imaging spectrum was produced. The averaged imaging spectrum was calibrated according to the sensitivity of the optical system and the spectrometer and was smoothed in the radial direction at each wavelength. Finally, the radial distribution of the emission intensity was determined by the inverse Abel conversion. This procedure was conducted for the eight wavelength ranges. The overall spectrum was obtained by connecting the eight individual spectra.

The overall spectrum of emission intensity at each radial position is shown in Fig. 4a for the nitrogen test flow. The spectrum is composed mainly of the first negative (1−) system and the Meinel system of N_2^+, and the first positive (1+) system and the second positive (2+) system of N_2. Although nitrogen is used as the working gas, the emission from NO, OH, NH, and CN, which are contained as the impurity, is seen to be prominent in the short wavelength range below 400 nm. Atomic carbon is considered to come from the contaminated wall, whereas oxygen and hydrogen are considered to originate from molecular oxygen and water vapor remaining in the ambient gas of the test section. This is because, at the moment of this measurement, there was no way to completely evacuated the test section so that the ambient gas was not replaced with the working gas before ignition of the ICP heater.

The overall spectrum of emission intensity for the air test flow is shown in Fig. 4b. In contrast to the nitrogen test flow, the most intense emission is seen to originate from NO, whereas the emission from N_2 and N_2^+ is considerably reduced. It is also noted that the emission from CN, OH, and NH is one of the major components of the overall spectrum in the short wavelength range below 400 nm. At $r = 32$ mm, the emission from OH is the most intense over the entire wavelength range. These results suggest that, to analyze the radiation spectrum observed in the test flow of the ICP wind tunnel, it is necessary to keep in mind that emission from impurities often affects the overall spectrum. When measuring the temperature using the spectrum fitting method, the neglect of such emission may reduce the accuracy of the estimated temperature.

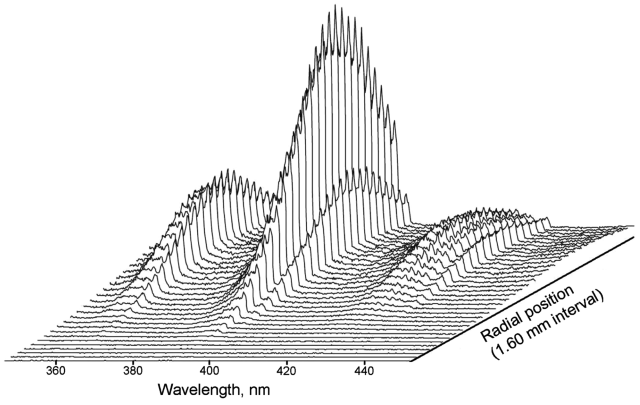

Fig. 3 Typical example of a radial imaging spectrum from 350 to 450 nm obtained in the air test flow.

B. Spectrum Fitting

The purpose of spectrum fitting is to measure the flow properties such as the temperature and the concentration of chemical components in the test section of the ICP wind tunnel and to examine the accuracy of the radiation code as well. When a satisfactory agreement between the observed and computed spectra is obtained, it can be concluded that the theory, the spectroscopic data, and the numerical procedure used to compute the spectrum are correct as a whole and that the flow parameters used to reproduce the observed spectrum coincide with those of the test flow.

In the previous study [11], the authors roughly measured the molecular temperatures in the test flow, finding that the flow is close to local thermal equilibrium. This is because the flow is low subsonic and the pressure remains sufficiently high in the absence of nozzle expansion (see Fig. 1). The molecular temperature was found to lie between 4000 and 6000 K at the center of the test flow. The computational fluid dynamic simulation of the ICP heater has also shown that the flow in the test section is close to thermal and chemical equilibrium [33]. Based on these results, numerical spectra were computed by SPRADIAN2 using the equilibrium chemical composition at temperatures from 3000 to 7000 K at every 50 K. The spectral matching criteria is to minimize the performance function

$$S = \sum_{i}^{N} [I_i / I(\lambda_i) - 1]^2 / N \tag{1}$$

where I_i and $I(\lambda_i)$ are the measured and calculated emission intensity at the wavelength λ_i, respectively, and N is the total number of the wavelength data points in the measured overall spectrum. However, as already described, the measured spectrum contains considerable emission from the impurities that are not included in the equilibrium composition for nitrogen and air. To take this into account, at each temperature, the emission intensity of the impurity was computed and added to the original numerical spectrum by changing its molar concentration until the performance function could be minimized. Because the molar concentration of the impurity is very small in general, the existence of the impurity was assumed to have no influence on the original equilibrium composition of the major species.

The final fitting results are shown in Figs. 5 and 6 for the nitrogen test flow and in Fig. 7 for the air test flow. As seen in Fig. 5, an excellent agreement between the measured and computed spectra can be obtained at the center of the test flow by setting the temperature to 5800 K in the calculation. In this case, based on the equilibrium composition of nitrogen at 10 kPa, the number density of

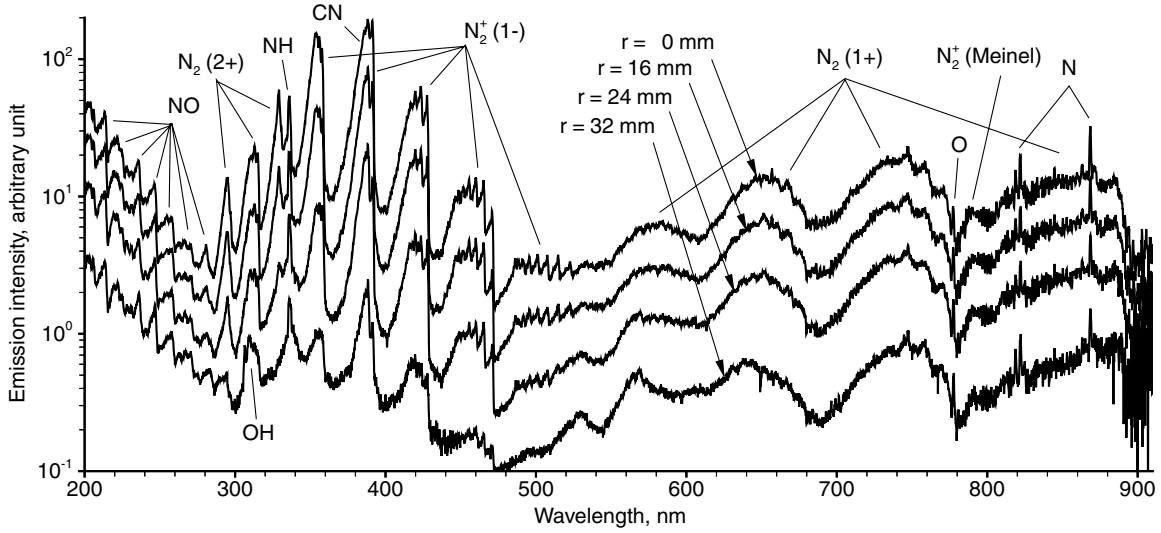

a)

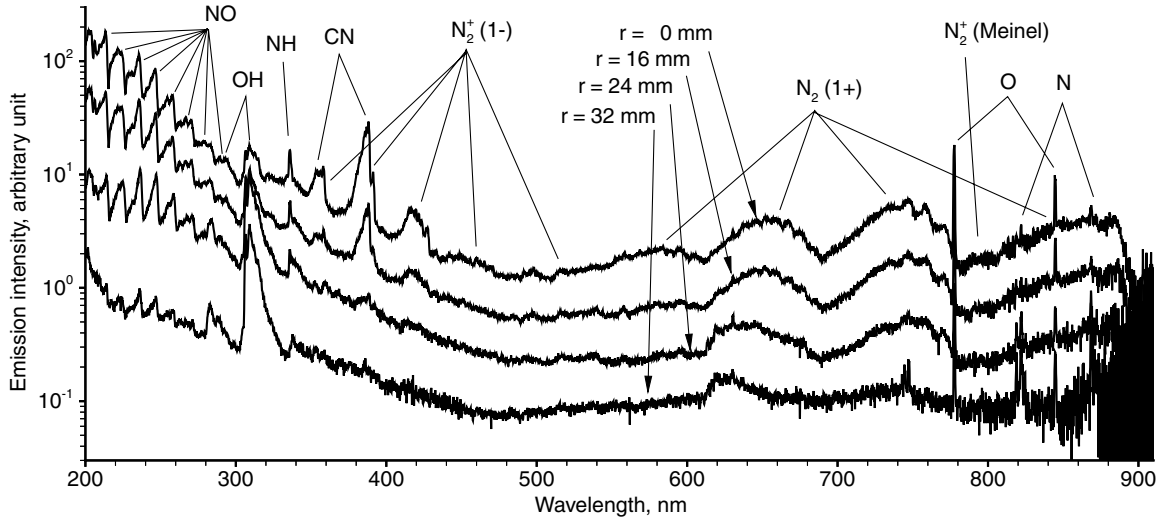

b)

Fig. 4 Overall spectrum of emission intensity at each radial position: a) nitrogen, and b) air test flow.

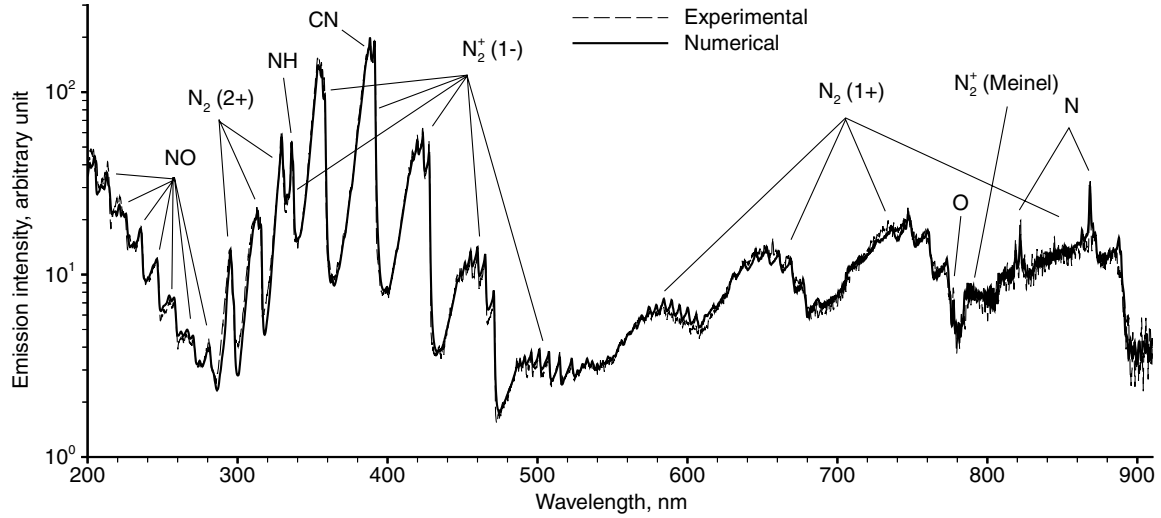

Fig. 5 Comparison between the numerical and observed spectra for the nitrogen test flow; radial position = 0 mm. Estimated temperature is 5800 ± 100 K.

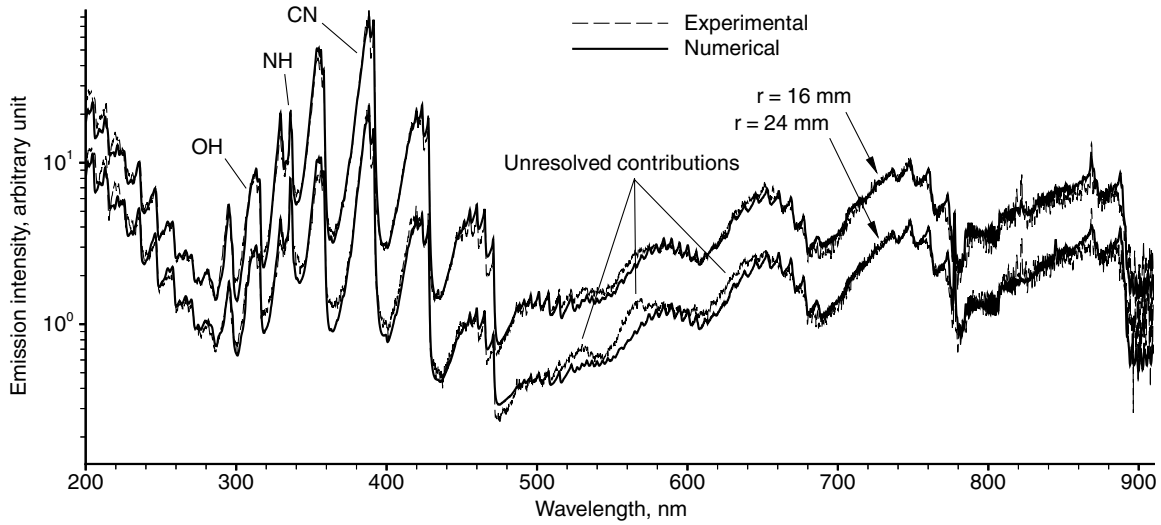

Fig. 6 Comparison between the numerical and observed spectra for the nitrogen test flow at outer radial positions; estimated temperature is 5500 ± 150 and 5200 ± 200 K for radial position = 16 and 24 mm, respectively.

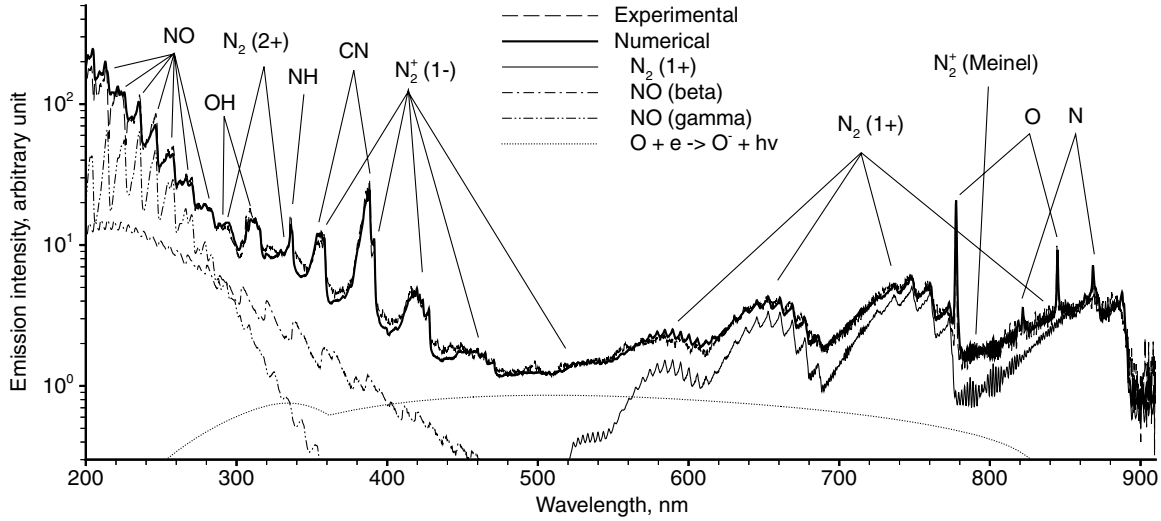

Fig. 7 Comparison between the numerical and observed spectra for the air test flow; radial position = 0 mm. Estimated temperature is 5600 ± 100 K.

N_2, N_2^+, N, and N^+ is set to 7.37×10^{22}, 1.07×10^{18}, 5.12×10^{22}, and 6.75×10^{18} m^{-3}, respectively, whereas that of O, NO, CN, and NH as the impurity is assumed to be 2.0×10^{21}, 8.0×10^{19}, 1.0×10^{17}, and 2.0×10^{17} m^{-3}, respectively. Agreement is degraded to some extent with increasing the distance from the flow center, as seen in Fig. 6. This is because the unresolved emission, the source of which has not been identified yet, increases in the wavelength range of 500–650 nm. In Fig. 7, the numerical spectrum for the air flow agrees well with the observed spectrum as well. In the air test flow, the emission caused in the reaction $O + e \rightarrow O^- + hv$ and that from the NO β system form the baseline of the spectrum in a wide wavelength range, as illustrated in Fig. 7. Most of the band spectra lying between 300 and 400 nm are those from the impurities.

The influence of the emission from OH, NH, and CN on the overall spectrum is illustrated in Fig. 8. Because the overall spectrum from 200 to 900 nm is used in the spectrum fitting procedure, the emission from these species does not have significant influence on the estimated temperature in the present measurement. However, when wavelengths observable in the measurement are limited, it is clear that the emission from CH, CN, and OH should be taken into account to accurately reproduce the spectrum, unless the impurities in the test section can be sufficiently eliminated.

In Fig. 9, a comparison is made between the numerical spectra computed by SPRADIAN version 1.6 (the old version) and SPRADIAN2 for the nitrogen test flow. Considerable differences are seen in the spectrum below 290 nm and between 570 and 700 nm, which are caused by the differences in the shape of the band spectra from NO and N_2, respectively. The NO spectrum ranging below 290 nm is composed of the β ($B^2\Pi \leftrightarrow X^2\Pi$), γ ($A^2\Sigma \leftrightarrow X^2\Pi$), δ ($C^2\Pi \leftrightarrow X^2\Pi$), and ϵ ($D^2\Sigma \leftrightarrow X^2\Pi$) systems. It is known that the spectrum from the $^2\Sigma \leftrightarrow {}^2\Pi$ transitions is poorly represented unless the spin splitting is considered [7]. Because the spin splitting for the γ and ϵ systems is accurately incorporated in SPRADIAN2, the agreement between the numerical and observed spectra is sufficiently improved. On the other hand, the spectrum above 550 nm mainly consists of the N_2 first positive system ($B^3\Pi \leftrightarrow A^3\Sigma$), which has moderate spin splitting. The poor agreement of the numerical spectrum obtained by the old version is attributed to inaccuracy in the transition probability included in the old database as well as neglect of the spin splitting. Improvement in the radiation code does not bring about noticeable differences in the spectrum from other transitions. In this study, because the overall spectrum from 200 to 900 nm is used to determine the temperature by the spectrum fitting method, the most probable temperatures deduced by using SPRADIAN and SPRADIAN2 are identical in most cases. However, uncertainty in the estimated temperature is reasonably reduced by using SPRADIAN2, because the experimental spectrum is better reproduced by SPRADIAN2.

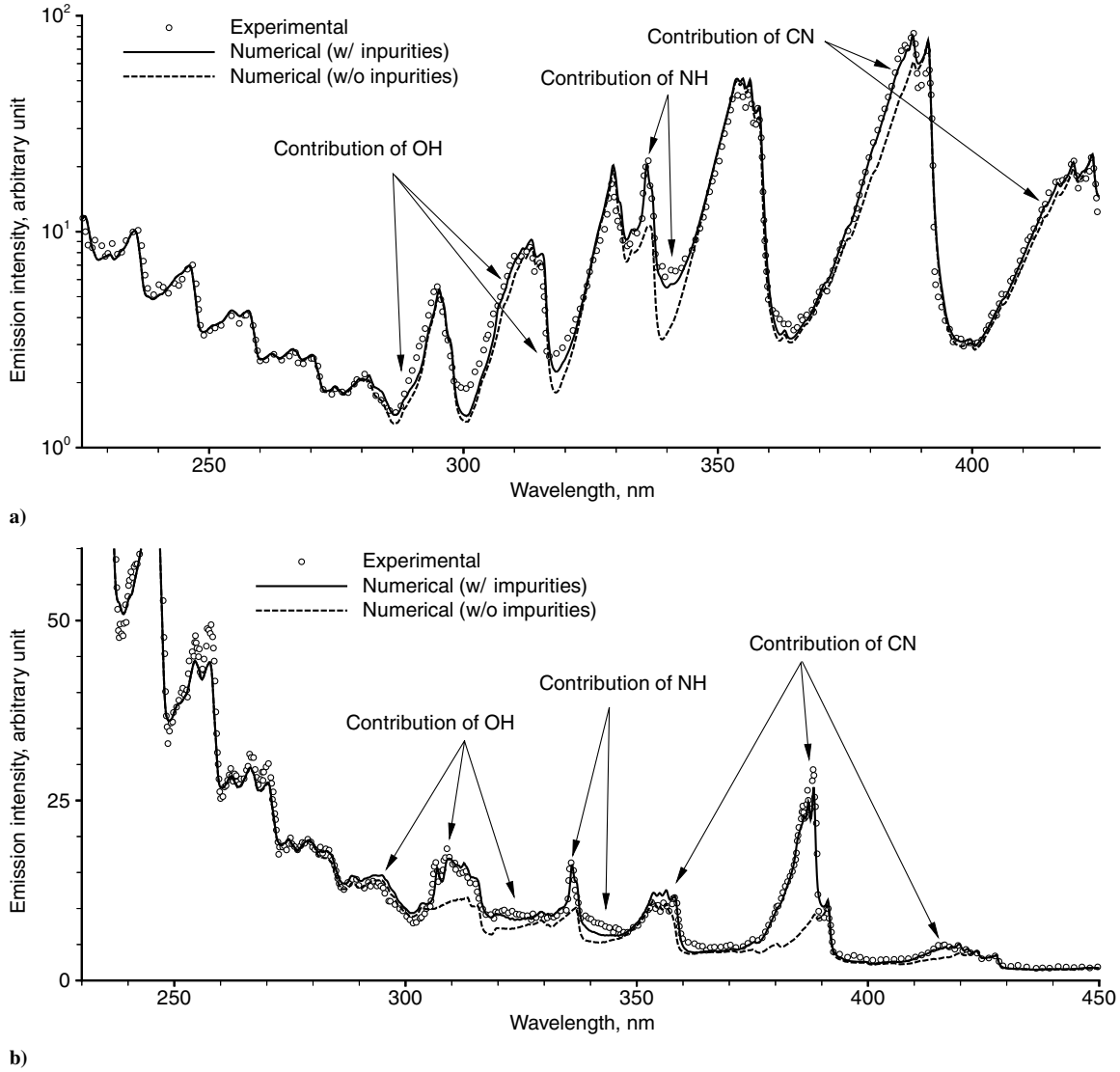

Fig. 8 Contributions of emission from impurities to the overall spectrum: a) working gas = nitrogen and radial position = 16 mm, and b) working gas = air and radial position = 0 mm.

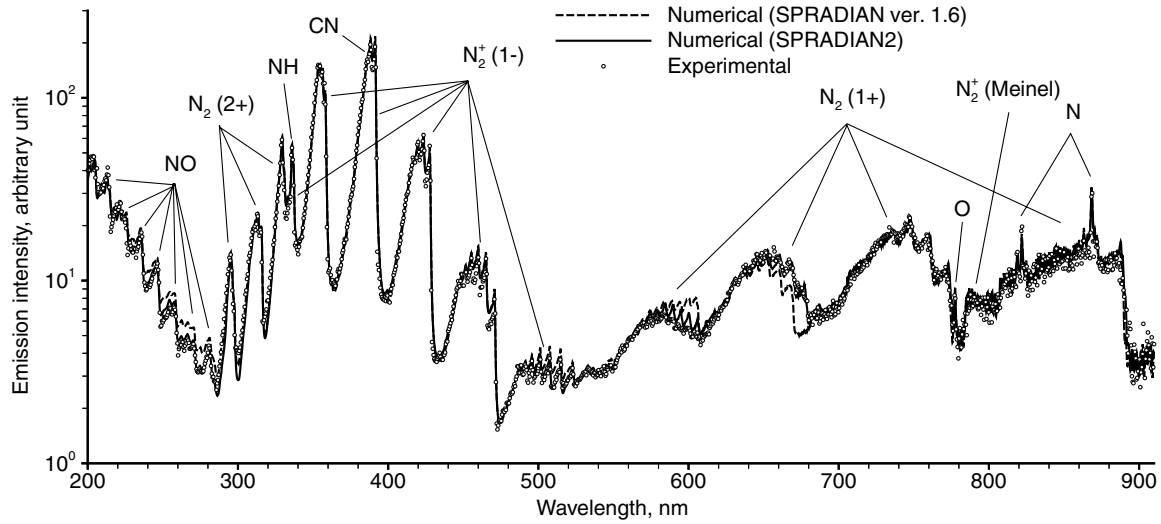

Fig. 9 Comparison between the numerical spectra computed by SPRADIAN and SPRADIAN2 for the nitrogen test flow; radial position = 0 mm.

In principle, the broad shape of the molecular band spectrum is determined by the relative intensity of the electronic–vibrational transition probability, or the Franc–Condon factor, which is determined from the intramolecular potentials of the upper and lower electronic states involved in the transition [9]. According to the references listed in Table 1, the spectroscopic constant used to define the intramolecular potential in SPRADIAN2 is so accurate that the spectrum shape can be calculated within a 10% error in this study.

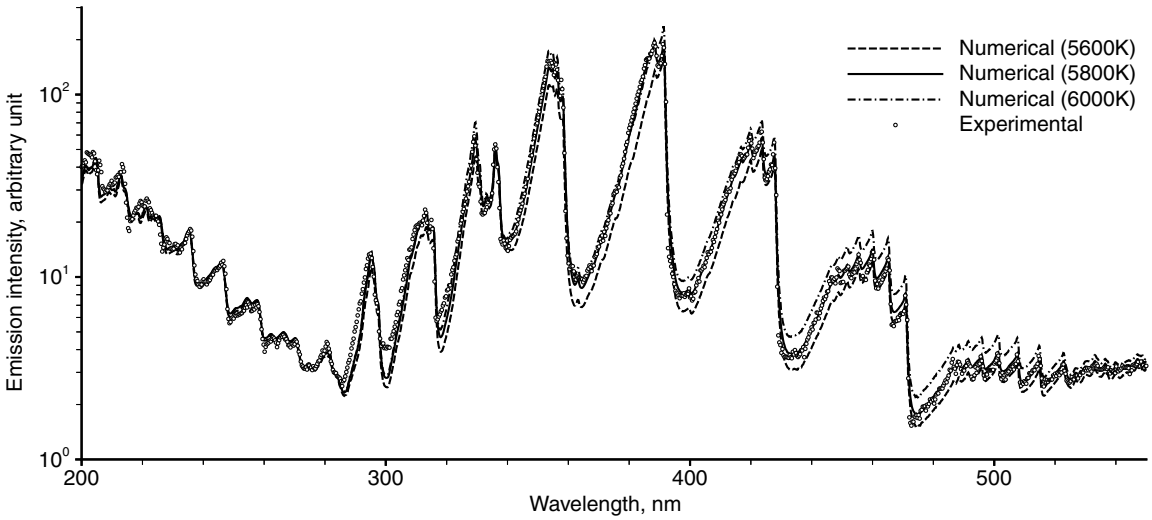

Fig. 10 Comparison between the numerical spectra calculated by setting the temperature to 5600, 5800, and 6000 K for the nitrogen test flow at the flow center.

Accordingly, the computed spectrum intensity, I_i in Eq. (1), has a 10% uncertainty, resulting in the corresponding uncertainty in the performance function. Neglecting the high-order terms, the uncertainty in the performance function is approximately given as

$$\delta S = \sum_{i}^{N} 2|I_i/I(\lambda_i) - 1|/N \times 0.1 I_i/I(\lambda_i) \tag{2}$$

To estimate the temperature from the measured spectrum, the optimum temperature is first searched for by minimizing the performance function given by Eq. (1), and then the uncertainty in the minimized performance function is calculated by Eq. (2). The sum of the minimized performance function and the uncertainty gives the tolerable maximum value of the performance function. Finally, the temperatures that can make the performance function less than the tolerable maximum value give the margin of error about the optimum temperature. In Fig. 10, a comparison is made between the numerical spectra calculated by setting the temperature to 5600, 5800, and 6000 K for the nitrogen test flow. It is seen that a small change in the temperature causes a considerable change in the spectrum shape, resulting in a significant increase of the performance function. In this case, the estimated temperature is 5800 K with a margin of error of ± 100 K.

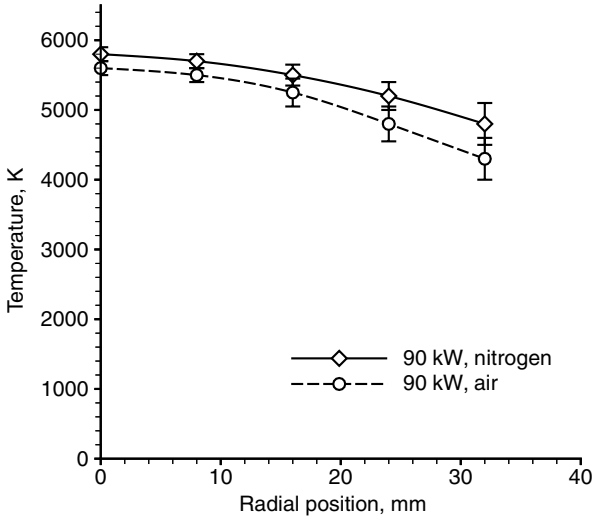

Fig. 11 Radial distribution of temperature in the nitrogen and air test flows.

C. Radial Distribution of Temperature and Chemical Composition

The determined temperature is plotted against the radial distance from the flow center in Fig. 11. The data are only available within a 32 mm radial distance, because emission from the test flow rapidly decreases beyond that. The temperature at the flow center is found to be slightly higher in the nitrogen flow than in the air flow. Because the test flow is low subsonic without acceleration by a nozzle, the kinetic energy of the flow is negligibly small compared with the thermal energy and the chemical potential. For this reason, the total enthalpy of the flow can be calculated as a function of temperature and pressure in the LTE condition. Based on this, the radial distribution of the flow enthalpy is calculated from the radial temperature distribution shown in Fig. 11. As a result, the total enthalpy averaged within a 25 mm distance from the center, which is the typical dimension of test pieces exposed to the test flow, is calculated to be 13.4 ± 1.0 and 13.7 ± 1.1 MJ/kg for the nitrogen and air flows, respectively. In contrast to this, the average flow enthalpy deduced from the thermal balance of the ICP heater is 17.7 ± 1 MJ/kg in both cases [6], which is approximately 30% higher than those determined from the spectroscopic results.

In [6], the energy put into the working gas is deduced by subtracting the thermal energy transferred to the coolant water from the electric energy supplied to the ICP heater. However, in a rough estimation, 5% of the thermal energy in the coolant water is lost to the piping system due to thermal conduction, resulting in a 10% overestimation of the flow enthalpy. In addition to this, the thermal energy of the heated working gas is lost to the flow duct and to the test chamber due to radiation. According to [11], the gas temperature in the ICP heater is as high as 10,000 K at the coil center, and 9000 K at a 40 mm downstream position from the coil center. Based on these results, in a rough estimation, the radiation loss in the upstream region of the test section amounts to 20% of the thermal energy initially put into the working gas. From this discussion, the average flow enthalpy at the test section is newly estimated from the thermal balance to be 12.9 ± 2 MJ/kg, which shows better agreement with the flow enthalpy obtained from the spectroscopic results.

Because the emission from the impurity is also reproduced in the spectrum fitting procedure, the radial distribution of its molar concentration is collaterally obtained in this study. The result for the nitrogen test flow is shown in Fig. 12, in which theoretical values for N_2 and N obtained by the equilibrium calculation are shown for comparison. Because the total intensity of the molecular band spectrum is proportional to the number density of the gas species, errors in the estimated molar fraction are proportional to errors in both the calculated and measured total intensity of the band spectrum. Errors in the calculated total intensity are proportional to errors in the electronic transition moment used to calculate the

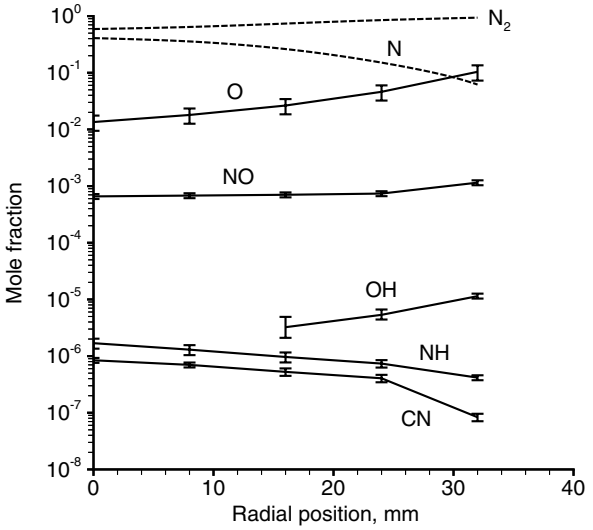

Fig. 12 Radial distribution of the impurities in the nitrogen test flow.

vibrational–electronic transition probability, which are taken from the references listed in Table 1 for each transition. On the other hand, errors in the measured total intensity change in relation to the intensity and shape of the overall spectrum. For example, because the total intensity of the band spectra from NO is relatively high in the overall spectrum, as seen in Fig. 5, errors in the measured intensity are small and expected to be less than $\pm 5\%$ at the center of the nitrogen test flow. In contrast to this, because the intensity of the atomic oxygen line at 777 nm is relatively low, and because this line is located in the close vicinity of the band head of the N_2 first positive system, the measured intensity of the oxygen line has a margin of error of $\pm 20\%$ at the flow center.

Although pure nitrogen is used as the working gas, the molar fraction of atomic oxygen amounts to 1.3% at the flow center and increases along with the radial position, as seen in Fig. 12. This is because molecular oxygen remains in the ambient gas of the test section due to an inadequate evacuation of the test section before ignition of the ICP heater. Likewise, the molar fraction of NO and OH increases along with the radial position, whereas that of NH and CN decreases conversely. These results suggest that the ambient gas in the test section should be replaced with the working gas if one wants to obtain much cleaner test flows. In response to this suggestion, the evacuation system of the ICP wind tunnel is currently under modification to reduce impurities for future heating tests.

V. Conclusions

The radiation code SPRADIAN has been improved by adding several chemical species, updating the database, and taking into account spin splitting to enhance the accuracy of the calculated spectral profile. The newer version, SPRADIAN2, has been successfully validated by comparing computed spectra with those observed in plasmas in local thermochemical equilibrium produced in the ICP wind tunnel. Using the imaging spectroscopy, the radial distribution of temperature as well as the molar concentration of chemical components was determined in the test section of the ICP wind tunnel by the spectrum fitting method. At the input power of 90 kW, the maximum temperature at the flow center is determined to be 5800 ± 100 and 5600 ± 100 K for the nitrogen and air flows, respectively, and the average flow enthalpy is estimated to be 13.4 ± 1.0 and 13.7 ± 1.1 MJ/kg, respectively. The spectrum fitting procedure used in this study is found to be useful to quantitatively assess the amount of impurities contained in the test flow as well. When nitrogen was used as the working gas, the molar fraction of atomic oxygen was seen to amount to 1.3% at the flow center due to an insufficient evacuation of the test section before ignition of the ICP heater. This suggests that the ambient gas in the test section should be replaced with the working gas when much cleaner test flows are required.

References

[1] Lochte-Holtgreven, W., *Plasma Diagnostics*, American Institute of Physics Press, New York, 1995.

[2] Griem, H. R., *Plasma Spectroscopy*, McGraw–Hill, New York, 1964.

[3] Fujita, K., and Abe, T., "SPRADIAN, Structured Package for Radiation Analysis: Theory and Application," The Institute of Space and Astronautical Science Rept. 669, Kanagawa, Japan, 1997.

[4] Fujita, K., Otsu, H., Yamada, T., and Abe, T., "Assessment of Radiative Reentry Environment around MUSES-C Capsule," *Journal of the Japan Society for Aeronautical and Space Sciences*, Vol. 51, No. 595, 2003, pp. 419–426. doi:10.2322/jjsass.51.419

[5] Fujita, K., Sato, S., Abe, T., and Ebinuma, Y., "Experimental Investigation of Air Radiation from Behind a Strong Shock Wave," *Journal of Thermophysics and Heat Transfer*, Vol. 16, No. 1, 2002, pp. 77–82.

[6] Ito, T., Kurotaki, T., Sumi, T., Fujita, K., Mizuno, M., and Ishida, K., "Evaluation of Surface Catalytic Effect on TPS in 110 kW ICP-Heated Wind Tunnel," AIAA Paper 2005-0189, Jan. 2005.

[7] Arnold, J. O., Whiting, E. E., and Lyle, G. C., "Line by Line Calculation of Spectra from Diatomic Molecules and Atoms Assuming a Voigt Line Profile," *Journal of Quantitative Spectroscopy and Radiative Transfer*, Vol. 9, No. 6, June 1969, pp. 775–798. doi:10.1016/0022-4073(69)90075-2

[8] Fujita, K., Sumi, T, Yamada, T., and Ishii, N., "Heating Environments of a Venus Entry Capsule in a Trail Balloon Mission," *Journal of Thermophysics and Heat Transfer*, Vol. 20, No. 3, 2006, pp. 507–516. doi:10.2514/1.18187

[9] Herzberg, G., *Molecular Spectra and Molecular Structure, Volume I: Spectra of Diatomic Molecules*, Van Nostrand Reinhold, New York, 1950, Chap. 5.

[10] Fujita, K., Mizuno, M., Ishida, K., Ito, T., Sumi, T., and Kurotaki, T., "Spectroscopic Diagnostics of Electrically Heated High Enthalpy Wind Tunnels," AIAA Paper 2005-0713, Jan, 2005.

[11] Fujita, K., Mizuno, M., Ishida, K., Ito, T., and Kurotaki, T., "Spectroscopic Measurement of ICP-Heated Wind Tunnel Plasmas," AIAA Paper 2004-2681, June–July 2004.

[12] Wiese, W. L., Smith, M. W., and Glennon, B. M., "*Atomic Transition Probabilities; Volume I: Hydrogen Through Neon*," National Standard Reference Data Series, National Bureau of Standards, Washington, DC, May 1966.

[13] Wiese, W. L., Fuhr, J. R., and Deters, T. M., "Atomic Transition Probabilities of Carbon, Nitrogen, and Oxygen: A Critical Data Compilation," Monograph No. 7, *Journal of Physical and Chemical Reference Data*, 1996.

[14] Herzberg, G., *Molecular Spectra and Molecular Structure, Volume IV: Constants of Diatomic Molecules*, Van Nostrand Reinhold, New York, 1979.

[15] Laher, R. R., and Gilmore, F. R., "Improved Fits for the Vibrational and Rotational Constants of Many States of Nitrogen and Oxygen," *Journal of Physical and Chemical Reference Data*, Vol. 20, No. 4, 1991, pp. 685–712.

[16] Gilmore, F. R., Laher, R. R., and Espy, P. J., "Franck-Condon Factors, r-Centroids, Electronic Transition Moments, and Einstein Coefficients for Many Nitrogen and Oxygen Band Systems," *Journal of Physical and Chemical Reference Data*, Vol. 21, No. 5, 1992, pp. 1005–1107.

[17] Luque, J., and Crosley, D. R., "Electronic Transition Moment and Rotational Transition Probabilities in CH. I. A $^2\Delta - X^2\Pi$ System," *Journal of Chemical Physics*, Vol. 104, No. 6, 1996, pp. 2146–2155. doi:10.1063/1.470970

[18] Luque, J., and Crosley, D. R., "Electronic Transition Moment and Rotational Transition Probabilities in CH. II. $B^2\Sigma^- - X^2\Pi$ System," *Journal of Chemical Physics*, Vol. 104, No. 11, 1996, pp. 3907–3913. doi:10.1063/1.471247

[19] Larsson, M., "A Theoretical Study of the Radiative Lifetime of the CH $A^2\Delta$ State," *Journal of Chemical Physics*, Vol. 79, No. 5, 1983, pp. 2270–2277. doi:10.1063/1.446077

[20] Ram, R. S., Bernath, P. F., and Hinkle, K. H., "Infrared Emission Spectroscopy of NH: Comparison of a Cryogenic Echelle Spectrograph with a Fourier Transform Spectrometer," *Journal of Chemical Physics*, Vol. 110, No. 12, 1999, pp. 5557–5563. doi:10.1063/1.478453

[21] Goldfield, E. M., and Kirby, K. P., "Ab Initio Studies of Low-Lying $^3\Sigma^-$, $^3\Pi$, and $^5\Sigma^-$ of NH. I. Potential Curves and Dipole Moment Functions," *Journal of Chemical Physics*, Vol. 87, No. 7, 1987, pp. 3986–3994. doi:10.1063/1.452901

[22] Kirby, K. P., and Goldfield, E. M., "Theoretical Study of the Radiative Properties of the Triplet States of the NH Radical: Transition Dipole Moments, Radiative Lifetimes, Photodissociation Cross Sections," *Journal of Chemical Physics*, Vol. 94, No. 2, 1991, pp. 1271–1276. doi:10.1063/1.460036

[23] Hay, P. J., and Dunning, T. H., Jr., "Polarization CI Wavefunctions: The Valence States of the NH Radical," *Journal of Chemical Physics*, Vol. 64, No. 12, 1976, pp. 5077–5087. doi:10.1063/1.432180

[24] Kuz'menko, N. E., Kuznetsova, L. A., Monyakin, A. P., Kuzyakov, Y. Y., and Plastinin, Y. A., "Electronic Transition Probabilities and Lifetimes of Electronically Excited States of Diatomic Molecules," *Soviet Physics; Uspekhi*, Vol. 22, No. 3, 1979, pp. 160–173. doi:10.1070/PU1979v022n03ABEH005425

[25] Schleicher, D. G., and A'Hearn, M. F., "The Fluorescence of Cometary OH," *Astrophysical Journal*, Vol. 331, Aug. 1988, pp. 1058–1077. doi:10.1086/166622

[26] Larsson, M., Siegbahn, P. E. M., and Agren, H., "A Theoretical Investigation of the Radiative Properties of the CN Red and Violet Systems," *Astrophysical Journal*, Vol. 272, 1983, pp. 369–376. doi:10.1086/161302

[27] Schoonveld, L., and Sundaram, S., "New Rotational and Vibrational Analyses of CN Violet System," *Astrophysical Journal*, Vol. 41, 1979, pp. 669–674. doi:10.1086/190636

[28] Knowles, P. J., Werner, H-J., Hay, P. J., and Cartwright, D. C., "The $A^2\Pi - X^2\Sigma^+$ Red and $B^2\Sigma^+ - X^2\Sigma^+$ Violet Systems of the CN Radical: Accurate Multireference Configuration Interaction Calculations of the Radiative Transition Probabilities," *Journal of Chemical Physics*, Vol. 89, No. 12, 1988, pp. 7334–7343. doi:10.1063/1.455264

[29] Gallusser, R., and Dressler, K., "Multistate Vibronic Coupling Between the Excited $^2\Pi$ States of the NO Molecule," *Journal of Chemical Physics*, Vol. 76, No. 9, May 1982, pp. 4311–4327. doi:10.1063/1.443565

[30] Langhoff, S. R., Bauschlicher, C. W. J., and Partridge, H., "Theoretical Study of the NO γ System," *Journal of Chemical Physics*, Vol. 89, No. 8, 1988, pp. 4909–4917. doi:10.1063/1.455661

[31] Cooper, D. M., "Theoretical Study of IR Band Intensities and Electronic Transition Moments for the β and δ Systems of NO," *Journal of Quantitative Spectroscopy and Radiative Transfer*, Vol. 27, No. 4, 1982, pp. 459–465. doi:10.1016/0022-4073(82)90080-2

[32] Cieslik, S., "Détermination Expérimentale des Forces d'Oscillateur des Principales Bandes des Systèmes β, γ, δ et ϵ de la Molécule NO," *Bulletin de la Classe des Sciences, Académie Royale de Belgique*, Series 5, Vol. 63, No. 11, 1977, pp. 884–901.

[33] Sumi, T., Fujita, K., Kurotaki, T., Ito, T., Mizuno, M., and Ishida, K., "Numerical Simulation of Inductively Coupled Air Plasmas," *Transactions of the Japan Society for Aeronautical and Space Sciences*, Vol. 48, No. 159, May 2005, pp. 40–45. doi:10.2322/tjsass.48.40